CHAPTER - 3

MAGNETIC PROPERTIES AND MICROSTRUCTURAL STUDIES.

MAGNETIC PROPERTIES AND MICROSTRUCTURAL STUDIES

SECTION-A

MAGNETIC PROPERTIES

INTRODUCTION

Magnetization is one of the fundamental parameters of ferrites. Besides magnetization, ferrites exhibit properties of switching and memory. The saturation magnetization, coercivity and remanance are studied with the help of 'hysteresis'. The magnetization is the magnetic moment per unit volume of material which is induced in it when placed in the external field. If magnetization is found in the absence of external field, it is called spontaneous magnetization. Ferromagnetic materials possess this spontaneous magnetization. The ferrites which are classified as ferrimagnetic materials, possess the spontaneous magnetization and exhibit almost all the properties of ferromagnets.

The saturation magnetization within the domain is the maximum, that can be achieved in the material at the given temperature. The origin of magnetization is in the aligning forces which arise from an internal magnetic field called "Weiss Molecular Field" in phenomenological description of magnetism[1]. However, quantum mechanics relates this to the Heisenberg's exchange forces.[2]

3.1. WEISS FIELD

Ferromagnetic materials possess permanent atomic moments arising from unpaired spins and these permanent atomic moments interact strongly with one another tending to cause parallel alignment of nearby moments. The moments of a large number of neighbouring ions are thus parallel even in the absence of applied

field. These domains of spontaneous magnetization exist in both single and polycrystalline material. The maximum moment within the domain determines saturation of it, at the given temperature.

Ferrite is the ferrimagnetic which contains two sets of moments A and B. All the A moments are aligned and so are all the B moments, but the resulting magnetic moment arises from the anti-parallel alignment of A moments with B moments. Neel[3] developed the theory of ferrimagnetism, which is described in chapter I.

3.2. EXCHANGE INTERACTION

The interaction between the spins can be explained, quantum mechanically by the equation,

$E = -2Je\ SiSj = -2Je.SiSj\ Cos\theta$ where, ... (3.1)

Je = Exchange integral

Si = Spin on 'i'th atom due to electron

Sj = Spin on 'j'th atom due to electron

θ = Angle between spins Si and Sj.

Je measures the extents to which the electronic charge distributions of two atoms overlap one another. The electrons under consideration spend a fraction of their time around the nuclei of both the atoms. For non-violation of Pauli's exclusion principle, electrons must be exchanged between the atoms. This direct exchange may be either positive or negative.

Slater and Bethe in 1933 have shown that in ferrimagnetic - spinels the ratios of atomic separation to diameter of 3d orbit are usually of the order of 2.5. Weak moderate positive interaction is suggested from direct exchange, yet experimental evidence favours a strong negative interaction between A and B sites.

When exchange integral is positive, parallel alignment of spins results of ferromagnetism and negative exchange integral - results in antiparallel alignment of spins, giving rise to antiferromagnetism. In absence of external magnetic field, such - ordered alignment of spins on A and B sites causes the resultant spontaneous magnetization in ferrites.

The magnetic ions are coupled through anions, by indirect exchange due to the transfer of electrons. The concept of indirect exchange was putforward by Cramers.[4] Further Anderson[5] developed it in the form of super exchange which is used to explain the magnetization in spinel ferrites.

3.3. HYSTERESIS

In order to discuss the suitability of electrical and electronic applications, it is necessary to describe the magnetiza - tion process in a quantitative manner[6].

If a demagnetized specimen is subjected to an external field, it gets magnetized. The magnetization will increase with the - strength of the applied field and reaches a saturation value at certain critical field. This curve OABC is called magnetization curve.

If the magnetizing field is reduced to zero and an increasing reverse field applied, the original magnetization curve OABC is not followed, but a lag(hysteresis) of the magnetization to the magnetizing field occurs. Increasing the reverse field leads to saturation in the reverse direction and if the field is again returned to the original direction, a complete cyclic loop - CDEFGC is obtained as shown in the figure 3.1. This relates - directly to AC applications. The area inside the loop is -

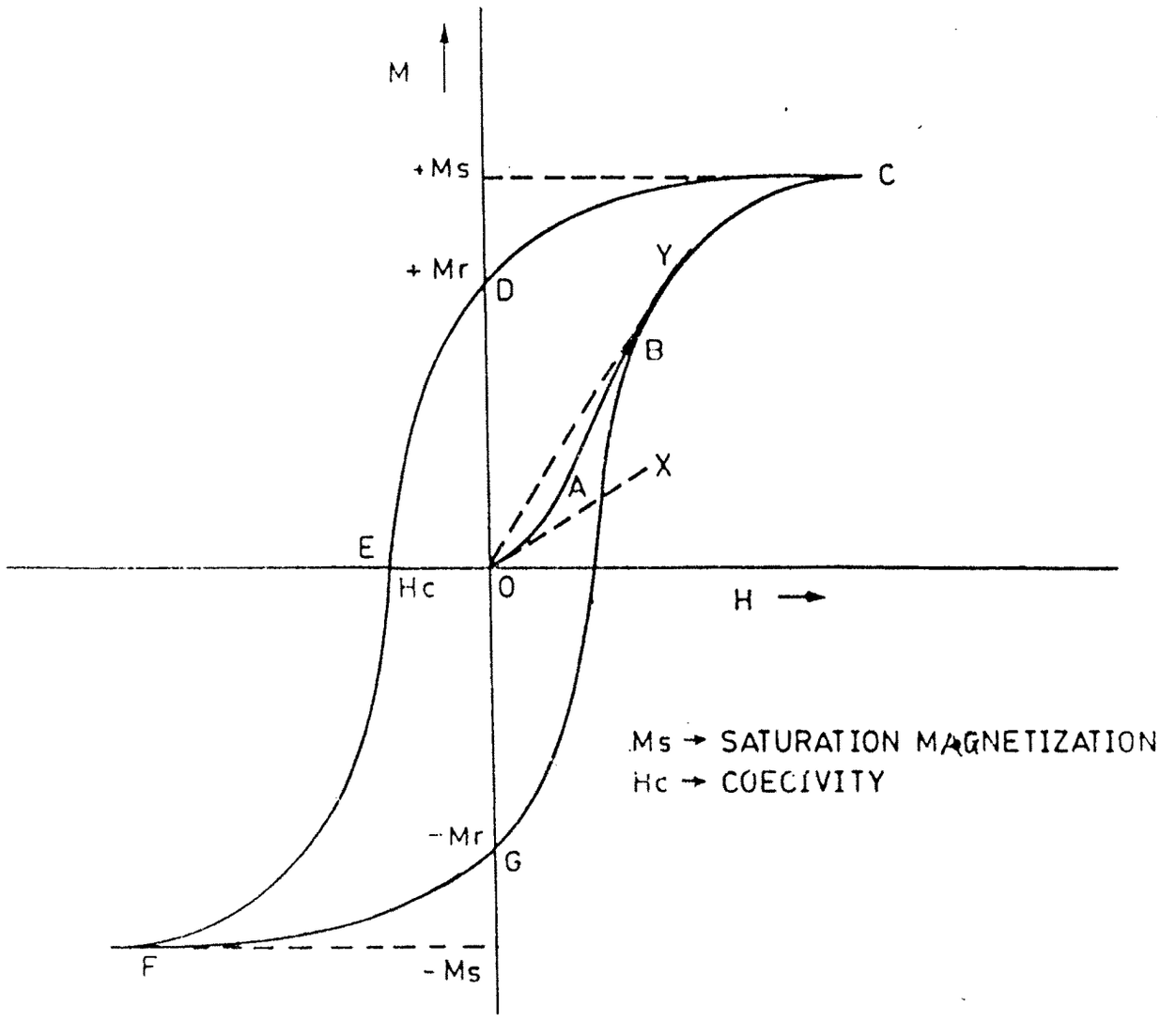

FIG. 3.1 MAGNETIZATION CURVE (OABC) AND HYSTERESIS LOOP (CDEFGC)

indicative of the losses occuring due to the traversal of the loop.

The slope of the tangent to the magnetization curve at the origin(OX) gives the magnitude of initial susceptibility Xo. The maximum susceptibility occurs at the knee of magnetization curve, determined by the slope of OY. The distortion factor required in magnetic recording applications are decided by initial susceptibility. Initial permeability can be measured by hysteresis loop, if the magnetic induction is plotted against magnetizing field.

The residual magnetization Mr at zero field is remanance or retentivity. The coercive field Hc is the required magnetizing field to demagnetize the specimen completely from retentivity. The saturation magnetization is given by the point 'C' of loop. The coercive field is found to vary from 10^{-1} to 10^{+3} oersteds.[7]

a) Experimental Technique

The saturation magnetization is measured, using high field loop tracer designed by CRK Murthy, Tata Institute of Fundamental Research, Bombay. The experimental set up is as shown in the figure 3.2. It consists of mainly three units viz.

i) C-core unit to feed the sample and to amplify the signal in core,

ii) Control unit to supply the power and

iii) Display unit to exhibit hysteresis loop on CRO and to carry out measurement with the help of digital multimeter.

The signal proportional to the magnetic moment of sample is supplied to the vertical plates of oscilloscope with requisite amplification and the signal proportional to the field applied, is fed to the horizontal plates of oscilloscope and all the preliminary adjustments of C-core unit and control unit are carried out,

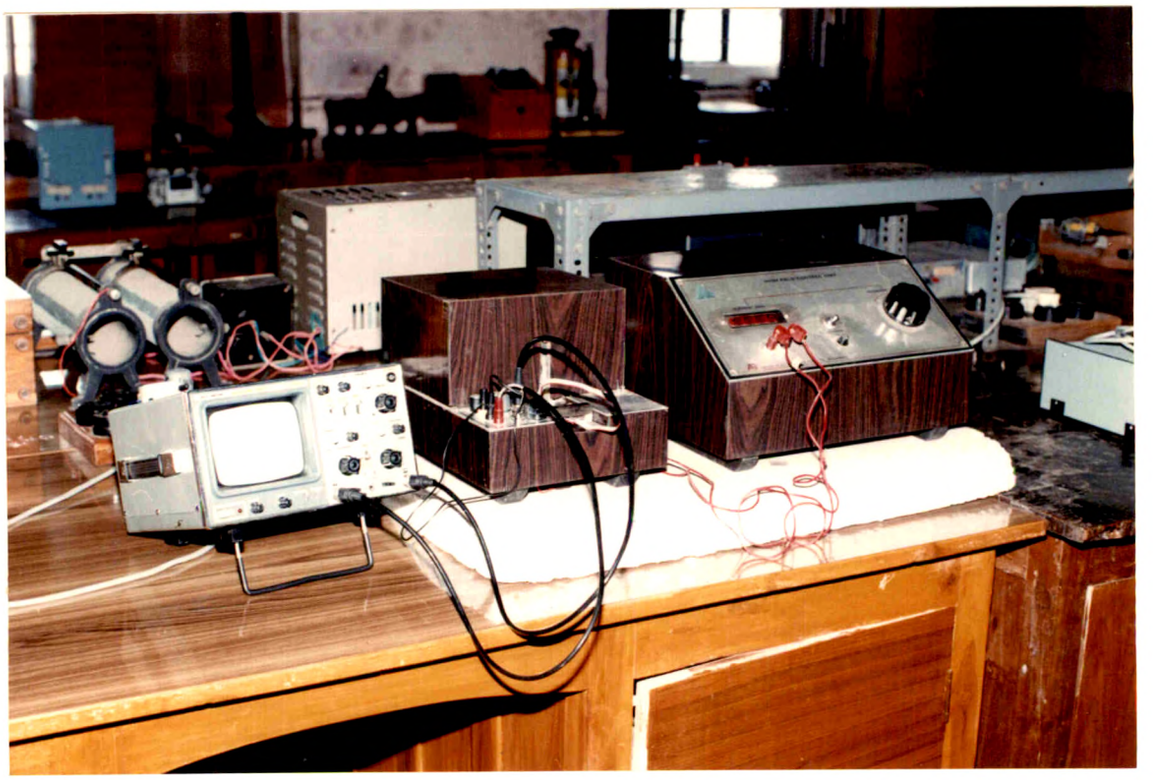

Fig. 3.2

EXPERIMENTAL SET UP FOR SATURATION MAGNETIZATION.

before it is calibrated by loading pure nickel sample between the pole pieces.

b) Calibration and Measurement of Saturation Magnetization

The vertical displacement on CRO is calibrated by loading pure nickel sample of mass 1.0611gms between the pole pieces of magnet in core unit. The selective range calibrator on oscilloscope is kept fixed on 0.5 volts per division for all the samples. The current in control unit of power supply is 100 mA. It gives the vertical displacement of 1.6cm. As the standard magnetization for nickel is 53.34 emu/gm, total magnetization of nickel is - 53.34 x 1.0611 = 56.5990 emu.

Therefore, calibration of height of hysteresis loop on vertical displacement is given by calibration factor = $\frac{56.5990}{1.6\text{cm}}$ = 35.37 emu/cm.

The vertical displacement for each sample is noted by introducing each pellet separately into the air gap between the pole pieces.

The saturation magnetization is calculated by the relation,

$$Ms = \frac{35.37 \times \text{height of hysteresis loop for a sample.}}{\text{Mass of sample.}} \text{ emu/gm.}$$

The magnetic moment per molecular formula unit in Bohr Magnetons is given by

$$n_B = \frac{Ms \times \text{Mol. wt. of unit cell}}{5585 \times d_a}$$ where,

d_a = actual density of sample in gm/cc.

c) Results and Discussion

The values of magnetization and magnetic moment observed in the experiment are tabulated in table 3.1 for the samples B_1 to B_7.

TABLE 3.1

RESULTS OF MAGNETIZATION EXPERIMENT AND POROSITY VALUES

System: $Zn_{0.3}Ni_{0.7+x}Mn_xFe_{2-2x}O_4$.

Content of Mn x	Vertical displacement in CRO in Cms.	Ms emu/gm	n_B observed in Bohr magnetons.	Theoritical n_B in Bohr Magnetons.	X-ray density dx. in gm/cc.	Actual density da. in gm/cc.	Porosity $P = \frac{dx-da}{da} \times 100$
B_1 0.0	1.9	46.35	3.873	4.4	5.5459	4.052	26.93
B_2 0.05	1.5	40.81	3.565	4.15	5.2395	3.877	26.004
B_3 0.1	1.9	41.844	3.734	3.9	5.2002	3.7966	26.99
B_4 0.15	1.6	38.24	3.672	3.65	-	-	-
B_5 0.2	1.7	35.47	3.482	3.4	4.9059	3.455	29.57
B_6 0.3	1.5	30.32	3.0207	2.9	5.2967	3.410	35.62
B_7 0.4	1.2	27.295	2.852	2.4	-	-	-

The pattern revealed by the samples in case of magnetic moment is that the initial magnetic moment of the first undoped sample decreases for x =0.05 concentration of Mn, then increases for x =0.1, with continuous decrease later on for any higher value of x.

N.L.Pakhomova and Christoph[8] have reported the value of magnetic moment for the $Zn_{.3}Ni_{.7}Fe_2O_4$ composition to be 4.22 Bohr - magnetons at 0^ok. Our value for the same sample at room temperature is found to be 3.873 Bohr Magnetons. The lower value can be justified due to higher room temperature in comparision with 0^oK.

It is observed similarly that, as content of Mn^{4+} increases the saturation magnetization decreases except with a small peak at x = 0.1. For any given value of x between 0 and 0.4, the magnetization is lower than the value at x =0.

The magnetization behaviour can be explained on the basis of cation distribution. Ti^{4+}, Zr^{4+}, Sn^{4+} substitutions in Ni-Zn - ferrites have been studied by A.R.Das et al.[9] Cu-Zn and Mg-Zn ferrite systems with Ti^{4+}, Zr^{4+} and Sn^{4+} substitutions are studied by S.R.Jadhav et al.[10] In these studies, it is observed that Ti^{4+}, Sn^{4+}, Ni^{2+} prefer B-sites and Zn^{2+} ions prefer A-sites. In the present system $Zn_{.3}Ni_{.7+x}Mn_xFe_{2-2x}O_4$, the general formula for - cation distribution may be given as,

$Fe_{1-p-q}Zn_pMn_q(Fe_{1+p+q-2x}Ni_{1+x-p}Mn_{x-q})O_4$ in which, cations in the bracket are at B-sites.

Gorter[11] has classified cations into different groups on the basis of electronic configurations. According to it, transition metal ions with $3d^3$ and $3d^8$ configurations prefer B-sites. These configurations belong to Mn^{4+} and Ni^{2+}.

Metal ion distribution in the system of $Mn_xFe_{3-x}O_4 (1 < x < 2)$ has been studied with the help of neutron-diffraction experiment[12] and it is suggested that Mn^{2+} goes to A-site whereas Mn^{3+} and Mn^{4+} prefer B-sites.

Considering the above facts, the cation distribution for the system $Zn_{.3}Ni_{.7+x}Mn_xFe_{2-2x}O_4$ can be given as, $Zn_{.3}Fe_{.7}(Ni_{.7+x}Mn_xFe_{1.3-2x})O_4$. This helps in illustrating cation distribution of our samples as

Sample	Mn concentration	Cation Distribution
B_1	0	$Zn_{.3}Fe_{.7}(Ni_{.7}Fe_{1.3})O_4$
B_2	.05	$Zn_{.3}Fe_{.7}(Ni_{.75}Mn_{.05}Fe_{1.2})O_4$
B_3	.1	$Zn_{.3}Fe_{.7}(Ni_{.8}Mn_{.1}Fe_{1.1})O_4$
B_4	.15	$Zn_{.3}Fe_{.7}(Ni_{.85}Mn_{.15}Fe_1)O_4$
B_5	.2	$Zn_{.3}Fe_{.7}(Ni_{.9}Mn_{.2}Fe_{.9})O_4$
B_6	.3	$Zn_{.3}Fe_{.7}(Ni_1Mn_{.3}Fe_{.7})O_4$
B_7	0.4	$Zn_{.3}Fe_{.7}(Ni_{1.1}Mn_{.4}Fe_{.5})O_4$

Magnetic moments of the ions Zn^{2+}, Ni^{2+}, Mn^{4+}, $Fe^{2+}(Mn^{2+})$, Fe^{3+} are 0, 2, 3, 4, (5) and 5 respectively. Theoritical magnetic moments (n_B) are calculated by applying the Neel's two sublattices model and the present cation distribution. Theoritical and experimental values of magnetic moments are tabulated in table 3.1. The values agree well with each other. It is shown in the figure 3.3.also.

The decrease of magnetization at x =0.05 and slight increase at x =0.1 can be explained differently. S.A.Patil et al[13] have studied the magnetic behaviour of Ti^{4+} substituted Mg-ferrites.

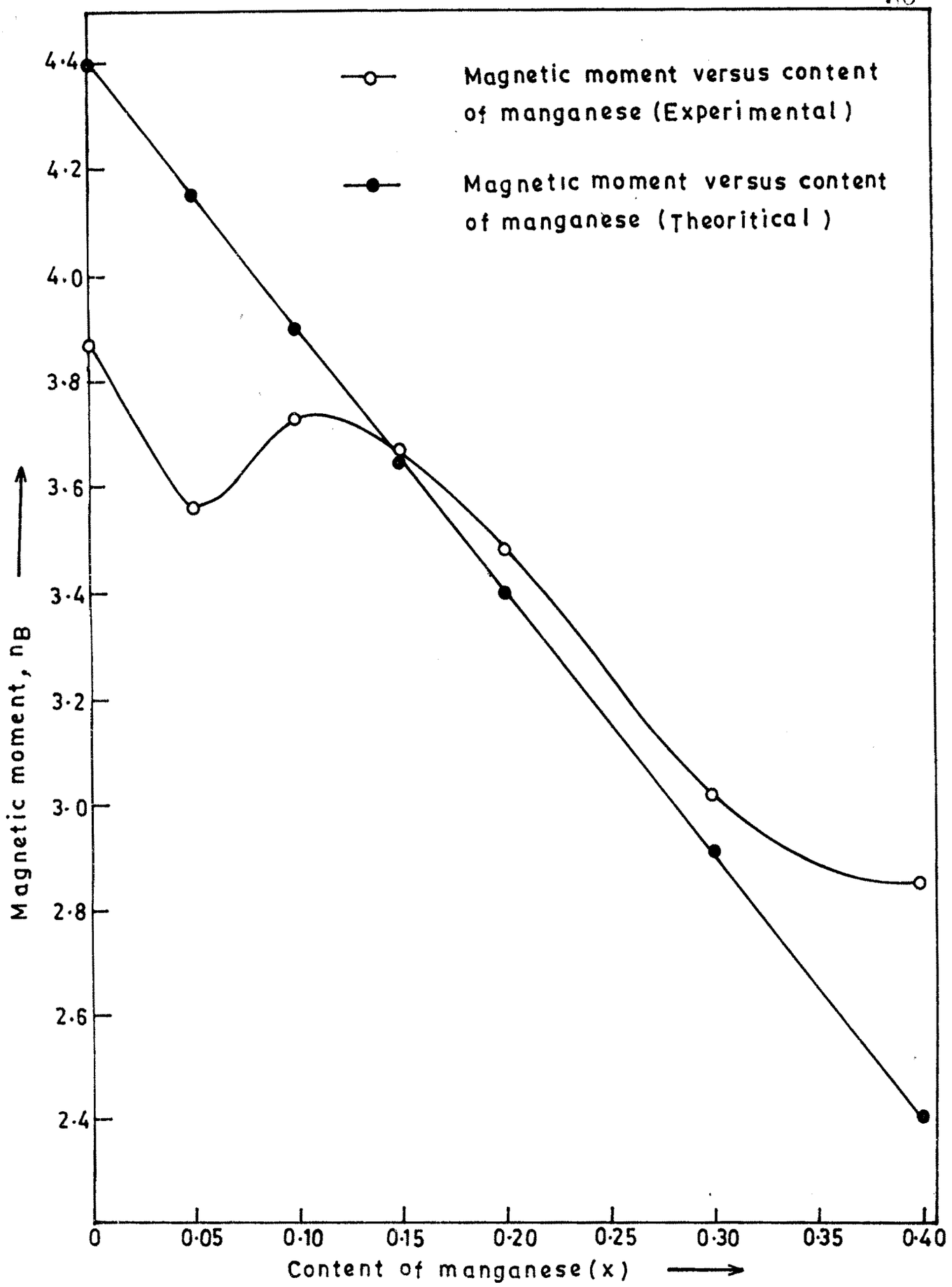

FIG. 3·3 – EXPERIMENTAL AND THEORITICAL MAGNETIC MOMENTS (n_B) VERSUS CONTENT OF Mn .

Magnetization decreases for Ti content less than 0.4, shows an increase at 0.4 and then continuously decreases for Ti content more than 0.4 in the system. The slight increase in magnetization is due to super paramagnetic behaviour of Fe^{3+} ions. - P.Kishan et al[14] have studied Li-ferrite substituted by Ti. They have observed a small increase in the hyperfine fields and have suggested that Fe^{3+} ion is responsible for the appearance of - super paramagnetic doublet contributing to hyperfine fields. Similar reason could be given to the increase of magnetization and magnetic moment in the present system for $x = 0.1$.

Table 3.1 also shows porosity and saturation magnetization with the variation of content of Mn. R.K.Puri et al[15] have - studied the normal and hot pressed $Mn_{.6}Zn_{.4-x}Ni_xFe_2O_4$ ferrites and reported that increase in strength of AB interaction is - responsible for the net increase in Ms. Higher values of Ms for hot pressed ferrites can be attributed to very low porosity of these ferrites, since larger porosity tends to decrease the - overall magnetization.

Magnetization of ferrites can be discussed with the help of microstructure. The presence of pores opposes the magnetization and motion of walls of domains. This reduces the magnetization - with increased pore concentration. When crystallites are large with negligible porosity, crystalline anisotropy reduces, making magnetization easy. Such behaviour can only be observed with the help of electron micrographs.

3.4. CURIE TEMPERATURE

In ferromagnetics the domains exist, which possess the magnetic moments or spins of atoms in parallel with each other.This

ordering is due to the presence of internal molecular field and is found to be maximum at $0^{o}k$. Therefore, the spontaneous magnetization is found to be maximum at absolute zero.

The temperature of the ferromagnetic substance, opposes this alignment and as temperature increases, spontaneous magnetization decreases. The critical temperature at which the spontaneous magnetization is lost by the ferromagnetic substance is called the curie temperature. When the temperature of ferromagnetic substance is greater than that of curie temperature, the disordered paramagnetic phase results. Thus curie temperature separates the disordered paramagnetic phase from the ordered ferromagnetic phase.

Ferrites exhibit the properties of ferromagnetics and curie temperature of ferrite depends on the distance of metallic ions on tetrahedral and octahedral sites according to the opinions of Gorter and Neel.

Rezlescu *et al*[16] studied the influence of the technique of preparation on various properties for mixed ferrites of Cu-Mn. Their study revealed the oxidation of $Cu^{1+} \dashrightarrow Cu^{2+}$ and their passage from tetrahedral to octahedral sites. The migration of manganese ion from octahedral to tetrahedral site is mainly responsible for the shift in curie temperature to lower temperature side.

Foresteir studied the $Ni_xZn_{1-x}Fe_2O_4$ to show the variation of curie temperature with the concentration of Zn. He related the variation of curie temperature to AB interaction. The nature of magnetizations at the intermediate temperature can very hardly be predicted.

a) Experimental Technique

The modified experimental set up, due to Laroia and Sinha[17] is shown in the figure 3.4. The soft iron piece and electromagnet were kept insulated from each other with the help of porcelein sheet. The electromagnet induced the magnetism in the soft iron piece kept inside the furnace. The sample of which curie temperature was to be determined, was fixed to this soft iron piece by slowly raising the position of the sample through the aperature at the base of the furnace and by using the phenomenon of attraction between magnet and sample. The mirror was used to see the sample pellet position, attached to this soft iron piece, which ensures that, pellet is magnetically attached to soft iron piece having induced magnetism.

At the bottom of furnace, a bed of cotton wool was spread so as to avoid the breaking of pellet when it falls. To measure the curie temperature, a chromel-alumel thermocouple was introduced in the furnace with its junction position very near to the position of the pellet. The other junction of the thermocouple was kept outside the furnace with a milli-voltmeter in the circuit to measure the temperature.

The temperature of the furnace was then raised by increasing the current in its coil, with the help of dimmer-stat. When the pellet fell down, the milli-voltmeter reading was noted and then converted to temperature with the help of calibration chart of chromel-alumel thermocouple. The procedure is repeated for other pellets of the same sample and average curie temperature of the sample is determined. This is repeated for other samples

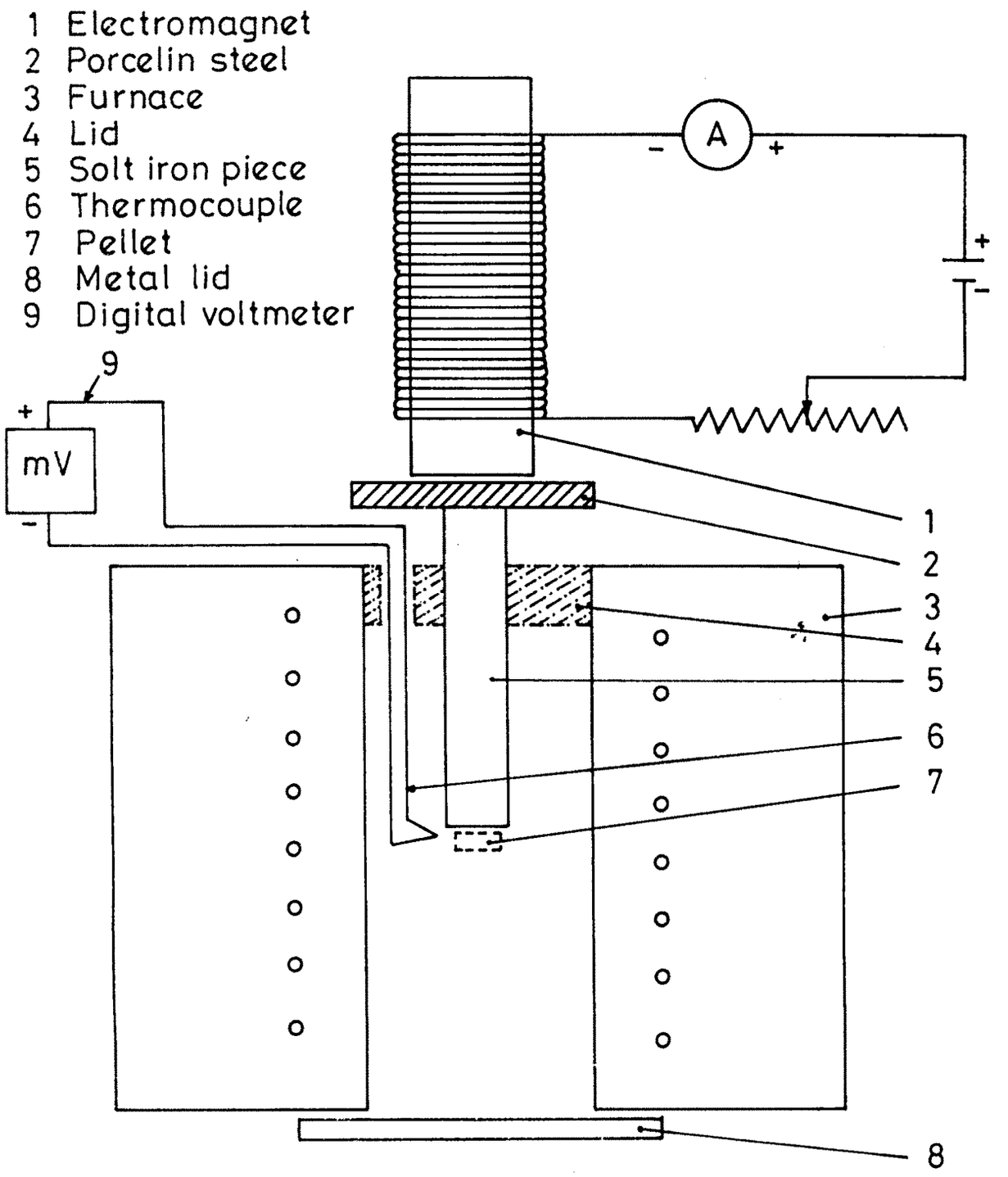

Fig. 3.4 Set up for determination of Curie Temperature .

and the results are tabulated in table 3.2.

TABLE 3.2

Sample	Curie temperature in degrees absolute
B_1: $Zn_{.3}Ni_{.7}Fe_2O_4$	603
B_2: $Zn_{.3}Ni_{.75}Mn_{.05}Fe_{1.9}O_4$	580
B_3: $Zn_{.3}Ni_{.8}Mn_{.1}Fe_{1.8}O_4$	642
B_4: $Zn_{.3}Ni_{.85}Mn_{.15}Fe_{1.7}O_4$	625.5
B_5: $Zn_{.3}Ni_{.9}Mn_{.2}Fe_{1.6}O_4$	560.5
B_6: $Zn_{.3}Ni_1Mn_{.3}Fe_{1.4}O_4$	559.5
B_7: $Zn_{.3}Ni_{1.1}Mn_{.4}Fe_{1.2}O_4$	514.25

b) Results and Discussion

The number of workers[18,19] studied the ferrites with substitutions like trivalent metals for Fe^{3+} ions and found that T_c decreased almost linearly as the concentration of substituted non-magnetic trivalent ion was increased.

In the case of $Ni_{1-t}Zn_tFe_2O_4$, the literature[20] gives the curie temperature of about 700°K for t =0.3. M.Haug and his co-workers[21] have recently reported the curie temperature of $Zn_{0.25}Ni_{.75}Fe_2O_4$ to be 729.5°K, with two percent error. N.L.Pakhomova and V.Christoph[8] have discussed the influence of competing interactions on the magnetic ordering of nickel-zinc ferrites and reported that $Ni_{.71}Zn_{.29}Fe^{2+}_{0.01}Fe^{3+}_{1.99}O_4$ has got the critical temperature of 695°K. However, for our sample B_1 the critical temperature is about 600°K and is found to be 636°K, in resistivity -

measurements. The observed low value in curie temperature can be attributed to preparation conditions and cation distribution.

For the small addition of $Mn_{0.05}$, the decrease in critical temperature is observed, similar to non-magnetic metal introduction in the ferrite. The rise in curie temperature for Mn =0.1 is in analogy with the rise in magnetization for this composition.For all the other samples the increasing composition of Mn behaves in a similar way as non-magnetic metals and can be attributed to the decreasing magnetic moments as seen in the table 3.1.

3.5. PERMEABILITY

The saturation magnetic moment is a function of a chemical composition and crystal structure. Permeability and losses are dependent on microstructural conditions. This is primarily true - as a.c. excitations produce rapid movement of domain walls and - since permeability is related to the ease of movement of these walls. The presence of imperfections in the ceramics structure reduces the permeability.

If only high permeability is required irrespective of losses, the grain boundaries act as impediments to domain wall motion. The fewer the grain boundaries, the larger the grains will be and higher the permeability. This has been observed in the case of Mn-Zn ferrites by Beer and Schwartz[22], Perduijn and Peloschek[23] and - Roess[24] but Guillaud and Paulus[25] showed it in the case of Ni-Zn ferrites first. This is in general consistent with metallic magnetic materials. The pores limit the domain wall movement. During the course of growing large grains, many pores are swept over by the grain boundary and remain inside the large grains. The -

intragranular porosity is more troublesome than the intergranular. Guillaud[26] showed in nickel-zinc ferrite that the permeability increased with grain size upto 15 μM, it decreases thereafter and this decrease was due to included porosity.

The intragranular pores, cracks, inclusions and second phases, residual strains are the imperfections that impede wall motion and these act as energy wells pinning the domain walls which require higher activation energy to detach.

a) Experimental Technique

The initial permeability was calculated from the inductance measurements with torroidal cores of N turns, using the formula

$L = 0.0046 \mu_i N^2 h \log_{10} (d_1/d_2)$ where, ...(3.2)

L = inductance in μH, h = height of core in inches,

d_1 = outside diameter in inches, d_2 = inside diameter in inches and μ_i is the initial permeability of the core.

LCR meter was used to measure the inductance of core at different temperatures, by keeping the wound torroid in the furnace. The temperature of furnace was measured by the chromel -alumel thermocouple. Along with inductance, Q values are measured at different temperatures of torroid, at fixed frequency of 1KHz.

The temperature co.efficient of initial permeability was evaluated using the formula given below,

Temperature co.efficient = $\mu_2 - \mu_1/\mu_1(\theta_2-\theta_1)$ for $\theta_2 > \theta_1$ .....(3.3)

where μ_1 is the a.c. initial permeability at temperature θ_1 and μ_2 is the initial permeability at temperature θ_2. The relative loss factor $\tan\delta/\mu i$ at room temperature is calculated for various samples.

The measurements of inductance L and dispersion factor D are carried out in Electronic Testing and Development Corporation, Peenya, Bangalore, with the torroidal samples with respect to frequency, using 4192 A Hewlett Packard LF Impedance Analyzer in the range 5Hz to 13 MHz.

b) Results and Discussion

The variations of initial permeability with temperature are as shown in the Fig.3.5 for 1KHz for our samples. The nature of the graph is similar in each case. Table 3.3 indicates the temperature co.efficients for each sample. The positive temperature co.efficient signifies the increase in the initial permeability - whereas negative permeability signifies the decrease in the permeability. The values of relative loss factor for 1KHz and 10KHz are tabulated in table 3.4.

Fig.3.5 shows sharp fall of initial permeability near curie temperature for B_1 sample and curie temperature can be measured accurately for it which agrees well with the values given by other methods. In other samples, addition of Mn^{4+} decreases the initial permeability. However, sharp falls are not observed in these - samples.

Permeability variation with the content of Mn^{4+} at a fixed temperature is shown in the fig.3.6. As the content of Mn increases from zero, initial permeability decreases and reaches a peak at $x = 0.1$. For further increase in x, initial permeability decreases. The increase or decrease in initial permeability is attributed to rise or fall in respective magnetization.

Fig.3.7 represents variation of initial permeability as a -

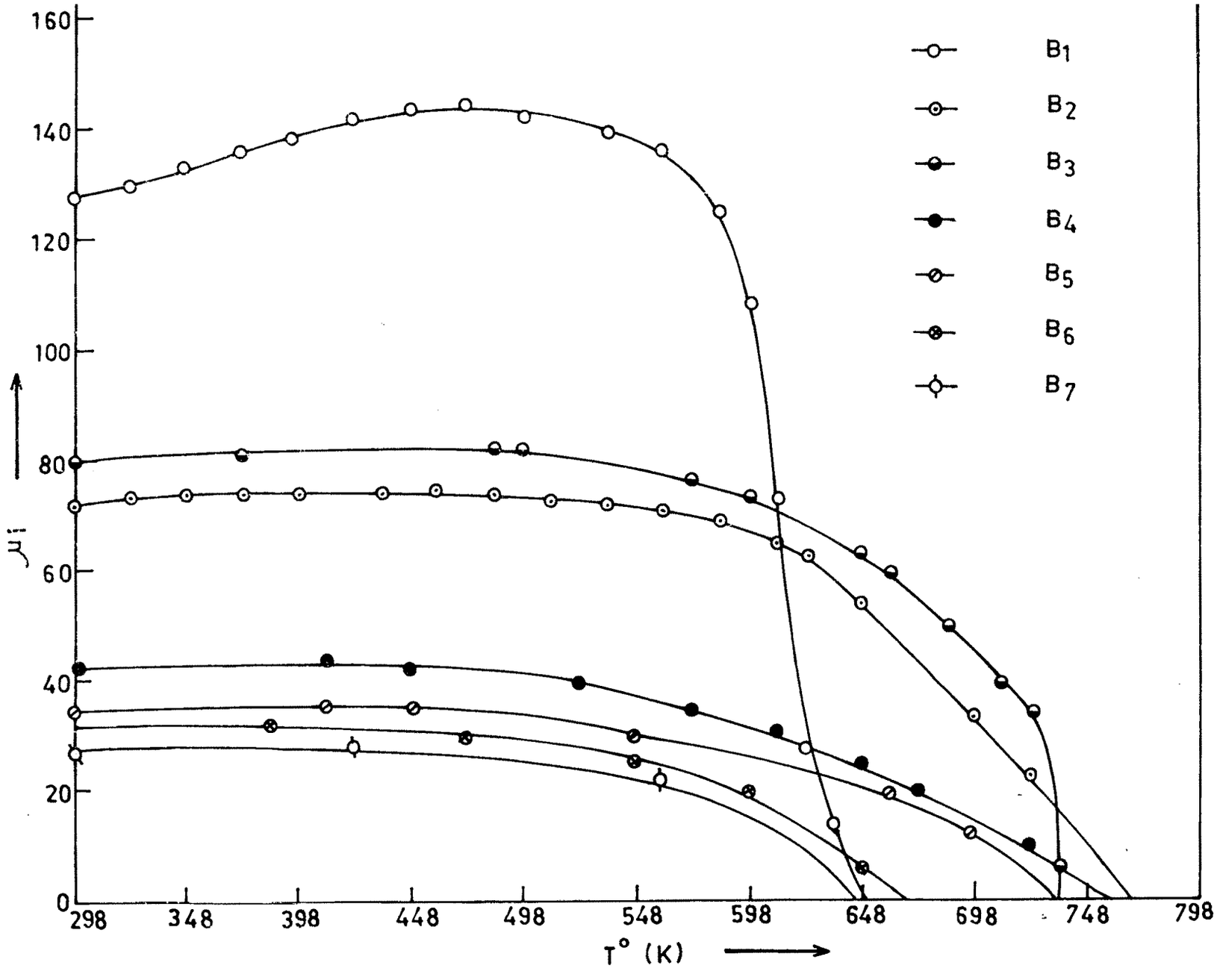

FIG. 3·5 — VARIATION OF INITIAL PERMEABILITY WITH TEMPERATURE FOR THE SERIES .

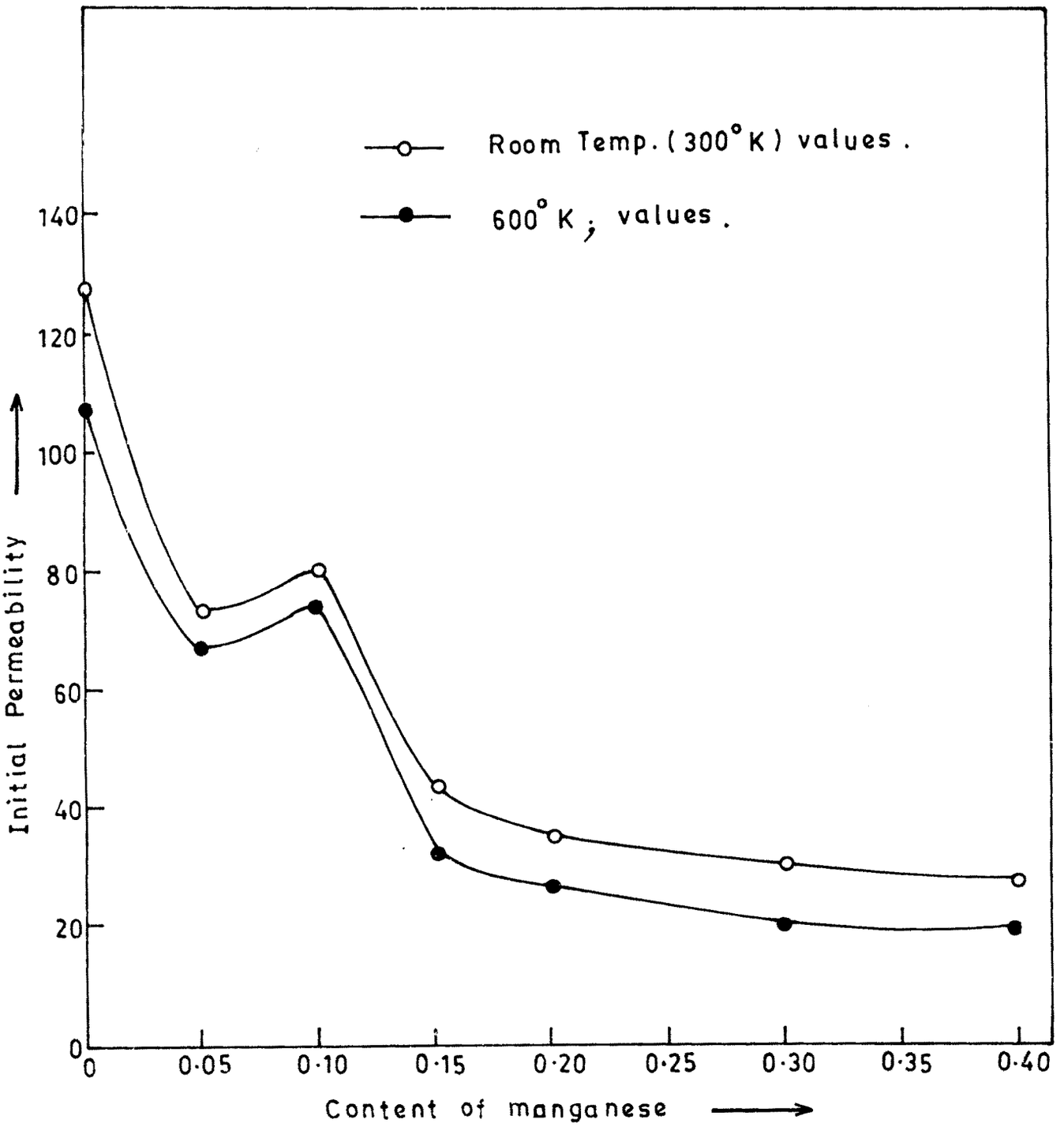

FIG. 3·6 — INITIAL PERMEABILITY WITH CONTENT OF MANGANESE AT 300 AND 600 DEGREES KELVIN .

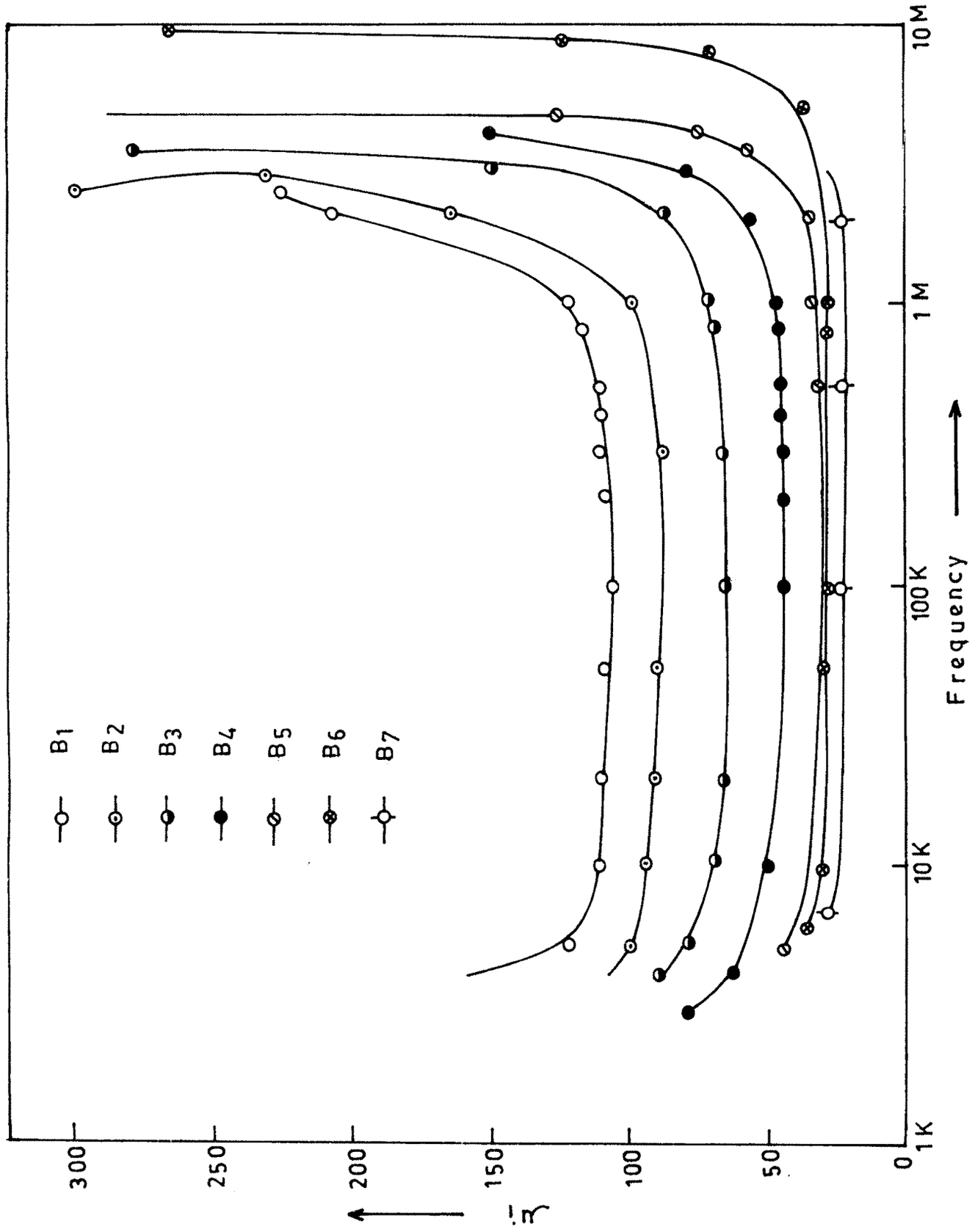

FIG. 3·7 — VARIATION OF INITIAL PERMEABILITY WITH FREQUENCY.

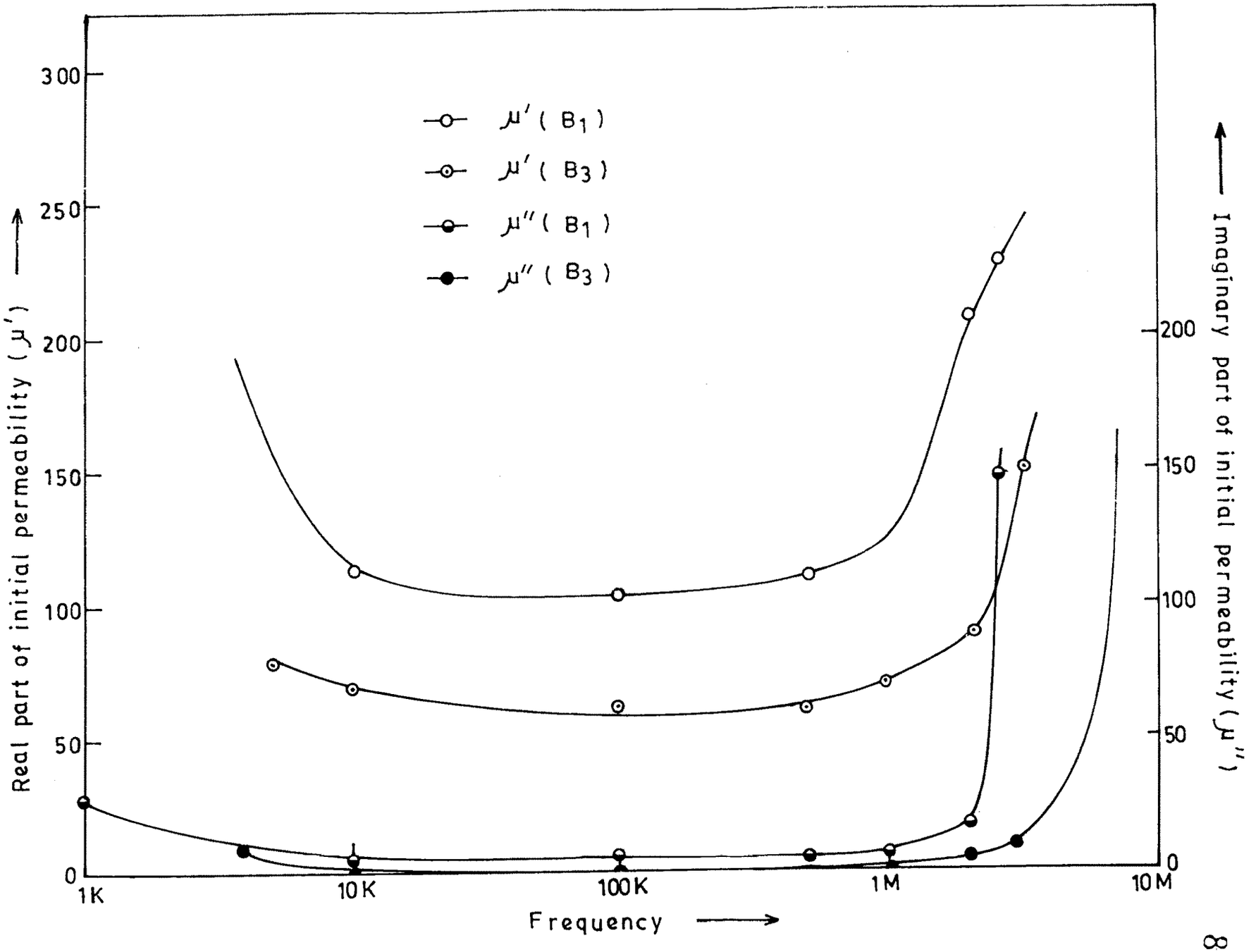

FIG. 3·8 — VARIATION OF REAL AND IMAGINARY PARTS OF INITIAL PERMEABILITY WITH FREQUENCY .

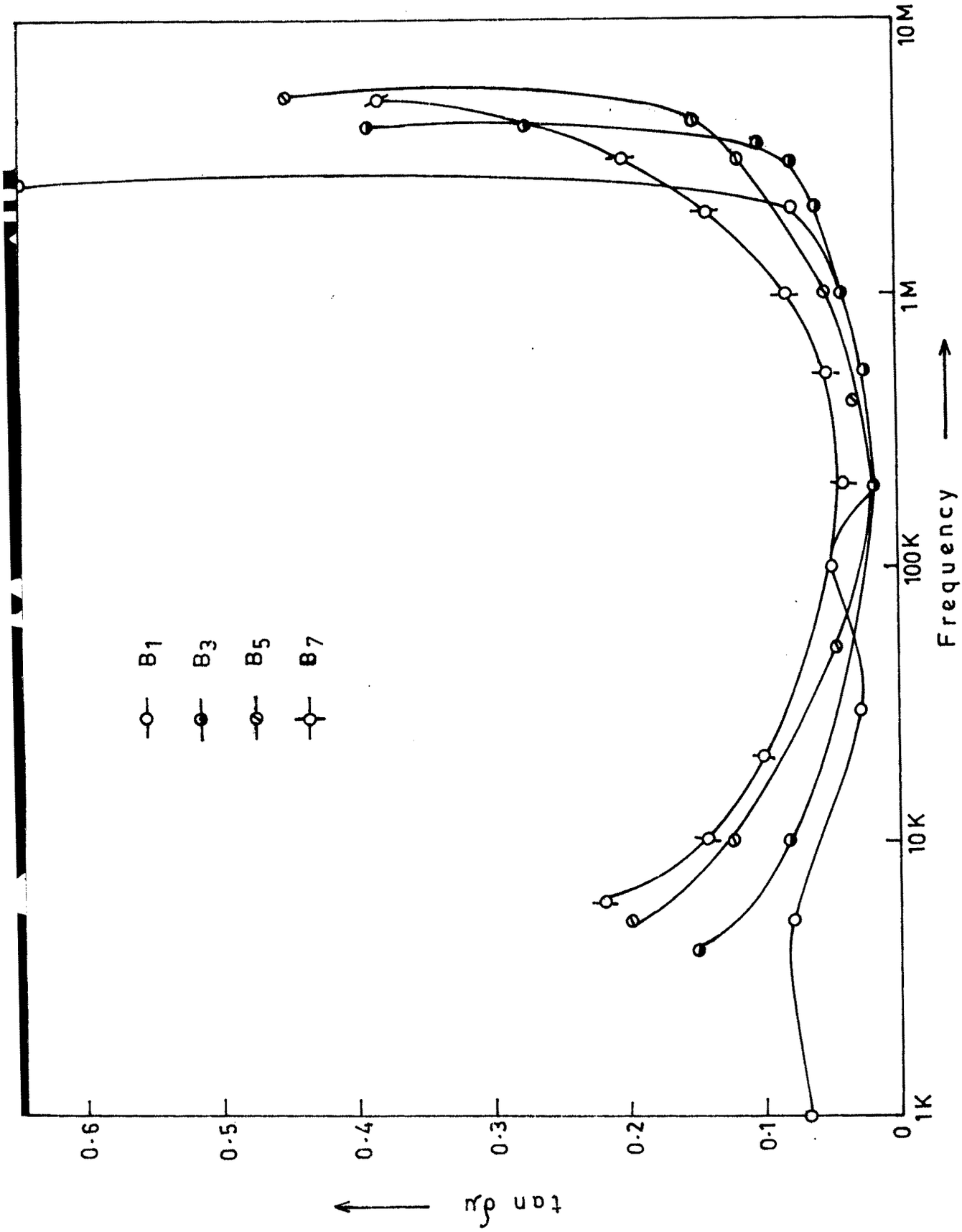

FIG. 3·9 — VARIATION OF tan δ_μ WITH FREQUENCY -

TABLE 3.3

TEMPERATURE CO.EFFICIENT AT 1KHz FOR DIFFERENT SAMPIES

Temperature in °K	B_1	B_3	B_5	B_7
298	-	-	-	-
348	9.33×10^{-4}	3.69×10^{-4}	3.91×10^{-4}	4.42×10^{-4}
398	6.68×10^{-4}	1.82×10^{-4}	-1.29×10^{-4}	1.22×10^{-4}
448	6.32×10^{-4}	5.38×10^{-5}	-00-	-1.22×10^{-4}
498	-8.36×10^{-5}	-1.02×10^{-4}	-1.05×10^{-3}	-8.66×10^{-5}
548	-6.29×10^{-4}	-5.41×10^{-4}	-1.82×10^{-3}	-1.21×10^{-3}
598	-4.49×10^{-3}	-1.43×10^{-3}	-1.96×10^{-3}	-3.80×10^{-3}
648	-19.5×10^{-3}	-2.65×10^{-3}	-3.99×10^{-3}	-14.42×10^{-3}
698		-5.80×10^{-3}	-8.05×10^{-3}	-19.32×10^{-3}
748		-17.65×10^{-3}	-9.14×10^{-3}	-
798		-16.72×10^{-3}	-13.6×10^{-3}	-

TABLE 3.4

RELATIVE LOSS FACTOR AT ROOM TEMPERATURE FOR DIFFERENT SAMPLES

Sample	Relative loss factor for 1KHz.	Relative loss factor for 10KHz.
B_1	1.92×10^{-3}	4.125×10^{-4}
B_2	4.70×10^{-3}	6.945×10^{-4}
B_3	4.710×10^{-3}	1.13×10^{-3}
B_4	12.5×10^{-3}	2.030×10^{-3}
B_5	18.76×10^{-3}	3.30×10^{-3}
B_6	21.2×10^{-3}	4.27×10^{-3}
B_7	28.7×10^{-3}	4.98×10^{-3}

function of frequency from 1KHz to 10MHz. All the samples show a similar behaviour. In the low frequency range permeability decreases upto 10KHz. In 10KHz to 1MHz region, it is almost independent of frequency and in the region 1MHz to 10MHz it increases with significant increase near the end of 10MHz.

Typical fig.3.8 shows the variations of imaginary part and real part of permeability with frequency for the samples B_1 and B_3. Variations of tanδ with frequency for various compositions are shown in the figure 3.9. We can discuss these observations in the following way.

For the fig.3.5, initial permeability increases with temperature for the sample with Mn content zero. It attains a maximum value and becomes very small at about $640^{o}K$ which is curie temperature of the sample. The effect of addition of Mn is to make permeability almost constant with temperature and suppresses the peaking behaviour. Density of the samples influences the bulk magnetic properties. The observed decrease in permeability can therefore be attributed to the decrease of density of the samples on addition of Mn.

Fomenko and Bashkieve[27] observed the increase in initial permeability on addition of Ti in Mn-Zn ferrite, which they attributed to compensation of anisotropy constant according to the relation $2Fe^{3+} \dashrightarrow Fe^{2+} + Ti^{4+}$. The increase in permeability in our system for $x = 0.1$ may be due to similar reason.

Peaks observed in initial permeability versus temperature plot in Ti and Zr substituted ferrites have been attributed to the compensation of negative value of anisotropy constant by many authors. In our sample B_1 for which $x = 0$, no sharp peak is

observed though the slight increasing trend of initial permeability is seen, with temperature. This may be due to the addition of Mn^{4+} which is magnetic in contrast to the non-magnetic Ti and Zr ions.

The physical mechanisms contributing to initial permeability are rotation of the magnetization and displacement of domain walls. For both contributions, expressions have been derived in the literature that relate initial permeability, anisotropy constant and saturation magnetization. Rado and Terris[28] studied the low frequency dispersion in ferrites attributing it to the domain wall motion. The decrease in the initial permeability is attributed to the less mobile domain walls in the low frequency region and in the region 1MHz to 10MHz, increase in initial permeability is attributed to more mobile domain walls.

Stopples[29] has stated that the permeability behaviour in the polycrystalline Mn-Zn ferrous ferrites is only weakly dependent on the frequency upto the MHz region. Buck and Ross[30] concluded that when the grain size of polycrystalline Mn-Zn ferrite is increased, the frequency dependence of permeability at frequencies below the ferromagnetic resonance increases.

Globus[31] has given the following approximate relation for initial permeability as, $\mu i = Ms^2 . dm / K_1$ where K_1 = anisotropy constant and dm = average grain diameter. Initial permeability is found to be depending on the preparation method, porosity present within the material and grain size.[32]

It can be concluded that the addition of Mn^{4+} impedes the motion of domain wall in low frequency region, making it almost

independent of frequency upto 1MHz region. Such behaviour has been observed in Zr^{4+} substituted Cu-Zn ferrite and in Sn^{4+} - substituted Ni ferrite.[33]

SECTION-B

MICROSTRUCTURAL STUDIES

INTRODUCTION

The increasing demands of ferrite materials in the rapidly developing electronic and telecommunication industries have made it necessary that intrinsic parameters should be studied in greater details. This will be helpful in the proper selection of material for any application. The combined efforts of science - and technology are required to realise the improvements in the ceramic products. The Scanning Electron Microscopy is one such powerful technique which is of immense importance in determining the intrinsic properties, based on grain size, porosity and inclusions.

3.6. MICROSTRUCTURE AND FERRITE

The relation between microstructure and property assumes a variety of forms in ferrites. The structures with large crystallites favour domain wall motion, high permeability and low - coercivity. Fine grained structure inhibits the wall motion and results in large retentivity and large coercivity. The proper grain orientation favours maximum BH_i value.

Improvement in any one relation most likely affects the other relations. Many investigators have tried such improvements in specific relations. Heister[34] and Paulus[35] have studied the -

magnetic properties via grain growth with SEM technique.

a) Electrical Properties

The grain boundaries act as sources of resistance. Guillaud[36] measuring the resistance of Mn-Zn ferrites, concluded that resistance is dominantly of that of grain boundaries. The grain boundaries represent lattice strain and disorders. They act as sources of impurities and usually prefer sites for inclusions. Heister stressed the need of uniform grain size for minimum losses.

The decrease in grain size enhances the porosity and it in turn being insulator, decreases the conductivity. At the sametime, firing temperature influences both grain size and porosity.

Van Uitert[37], LongKla[38] and others observed that resistance increases in spinels on the addition of impurities. Mobility[39] of charge carriers is found to be more for a.c. rather than d.c.

b) Magnetic Properties

The large crystallites without pores or imperfections and with small anisotropy possess high permeability. This is due to the - highly mobile domain walls. The domain walls increase in size and oscillate more freely as the grain size increases and domain wall relaxation frequency and maximum losses, shift to lower values with increasing grain size.[40]

Perduijn[41] and many other investigators have shown the linear relationship between the permeability and average grain diameter.The grain diameter is related to the sintering temperature and other relevant factors such as raw materials, purity and chemical homogeneity. The experimental results[42] of B-H loop in case of Ni-Zn ferrites suggest that magnetic flux density and coercive force are

independent of porosity and grain size and Besenicar et al[43], studied the microstructural properties by Mossbauer spectra of Fe at room temperature. In general, single crystals are preferred for constant or slow varying field but for high frequencies, polycrystalline structure is preferable due to low losses in such structure.

3.7. ASPECTS OF MICROSTRUCTURE

The knowledge of characteristic elements of microstructure and its control is necessary in order to extract optimal properties from a specimen. These characteristic elements in ferrite are grain size, their orientation, porosity and inclusions. The final microstructure of the ferrite is due to the sintering process. Hence, in the following, we discuss sintering, grain growth, exaggerated grain growth and porosity in brief, as the aspects of microstructure.

a) Sintering

The heating of a powder compact to an elevated temperature at which mobility of grain boundaries is high, reduce the free energy associated with the grain boundaries. This initiates formation of a neck between the neighbouring particles. The growth of neck is controlled by diffusion process during sintering. The growth of grain actually starts when the density is about 60 percent of theoritical density. Moving grain boundaries sweep away the pores and some of the pores may be swallowed by the grains. The pores inside the grain are removed by diffusion of vacancies.

Sintering and densification involve the diffusion process of vacancies from pores to grain boundaries where vacancies are -

annihilated. This initiates migration of ions by grain boundaries to the pores producing shrinkage. This transport mechanism is - essential for densification and requires sufficiently high energy to be associated with surface of particles which in turn demands - small size of spherical particles in reaction. The surface energy per unit volume of a spherical particle is, $E_s = 6\gamma/D$ .....(3.4) where γ = surface tension and D = diameter of the particle. The concentration of vacancy under a surface of radius r, is given by Kelvin as, $Cr = Co\ Exp(2\gamma a^3/rKT)$ where, ...(3.5)

Cr = concentration of vacancy under a surface of radius r,

Co = concentration of vacancy under flat surface,

a^3 = volume of vacancy and γ = surface tension.

For good quality ferrite, introduction of atmosphere having controlled amount of oxygen during sintering is essential. The - atmosphere is either air or oxygen while soaking, but oxygen par - tial pressure has to be changed during cooling, so that ferrite is in equilibrium with atmosphere and no oxidation reduction of Fe^{2+} ions takes place as, $Fe^{2+} + \frac{1}{4} O_2(g) \rightleftarrows Fe^{3+} + \frac{3}{8} V_c + \frac{1}{2} O^{2-}$ This controls the amount of Fe^{2+} ions and does not allow to form the gradient of Fe^{2+} from surface to the interior.

b) Grain Growth

The source of driving force for grain growth is grain boundary. As grain size increases, the energy of boundary decreases - and boundaries move toward the centre of curvature. The grain growth[44] is given by, $D-D_o = kt^n$ where, ...(3.6)

D_o = original particle size, k = temperature dependent factor,

t = time and n = grain growth exponent = 1/2 or 1/3. -

The presence of impurities in the grain boundaries hinders the grain growth. The grain growth occurs until the ratio of - diameter of inclusion to the volume fraction is equal to the - critical diameter of grain. Further growth is inhibited. The lowest possible porosity and full densification can be obtained by promoting rate of sintering and by using fine particles. - Reijnen[45], Nabarro[46] and Herring[47] are the main research-workers in the field of microstructure of ferrites.

c) Exaggerated Grain Growth

The grain size cannot be controlled completely in the sintering process, unless very pure raw materials are used. After reaching a critical grain size, few grains grow rapidly at the cost of others, constituting what is known as discontinuous growth. It leads to duplex structure. This is favoured if impurities and inhomogeneity exist[48] and it can be related to inclusions.[49]

d) Porosity

In ceramics, prepared by powder compaction and sintering, porosity is always present. High rate of sintering with small particle size reduces the porosity appreciably. Pores pin domain walls and can reduce the permeability. The grains free from pores lead to very high permeability.

The poor rate of sintering is the cause of microstructure - with large pore concentrations. The optimum rate of sintering is achieved when the condition, $D_c C_c = D_o C_o$ .....(3.7) is satisfied, where D_c is diffusion constant of cation vacancies. D_o is diffusion constant of oxygen vacancies, C_c is the bulk -

concentration of cation vacancies and C_o is bulk concentration of oxygen vacancies. Discontinuous grain growth is favoured for no pore growth. The low porosity and small grain size combination is very difficult to realise in practice. However, such combinations are achieved by using hot pressing technique.

3.8. EXPERIMENTAL TECHNIQUE

Scanning Electron Microscope is the most advanced instrument, used in the study of metallography and microstructure. It possesses high magnification and resolving power with the ability to form three dimensional image.

The micrographs of our samples are obtained to characterise their microstructure with the help of S.E.M, Cambridge Steroscan-S-250 MK II. This facility is made available to us, by R.S.I.C. Nagpur University, Nagpur.

The pellets used for this purpose are coated with a paste of gold and are allowed to dry for about half an hour. Such a pellet is inserted in its place specially designed for it, in the machine which is switched on to prepare a vacuum pressure for about 45 minutes. The different surfaces of the pellet can be scanned and photograph of the selected surface is taken with the help of - camera. These micrographs are displayed in the figure 3.10.

3.9. RESULTS AND DISCUSSION

These micrographs reveal the following important features.

1. The grain size slowly increases upto Mn content 0.1 and then decreases with Mn concentration.
2. The porosity increases with increase of Mn content. X-ray diffraction studies reveal the range from 26 to 35 percent of porosity and it supports the above observation.

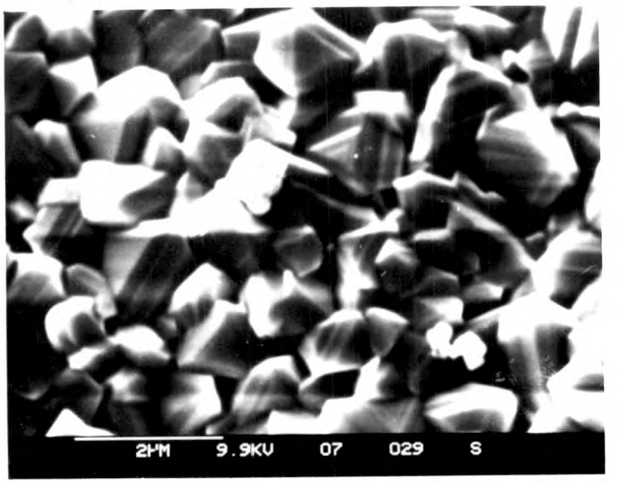

B_1

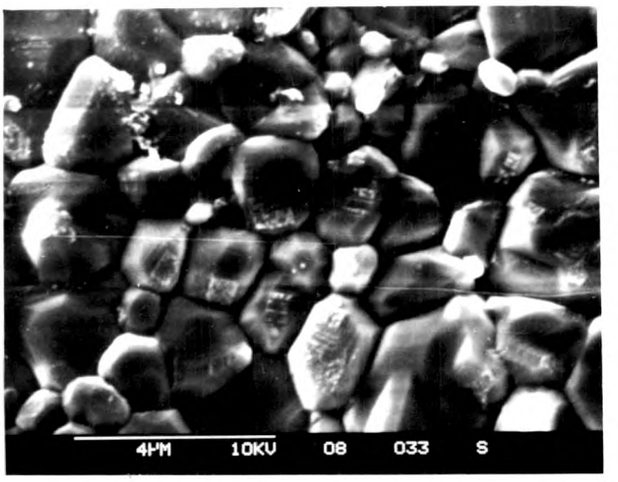

B_2

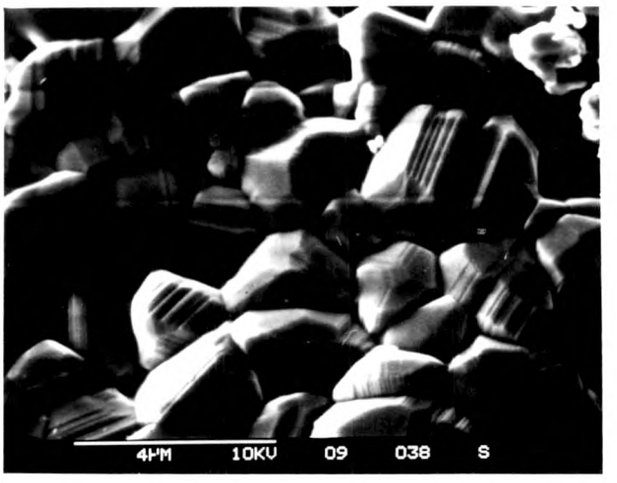

B_3

Fig. 3.10(a)

MICROGRAPHS OF SAMPLES B_1, B_2 AND B_3

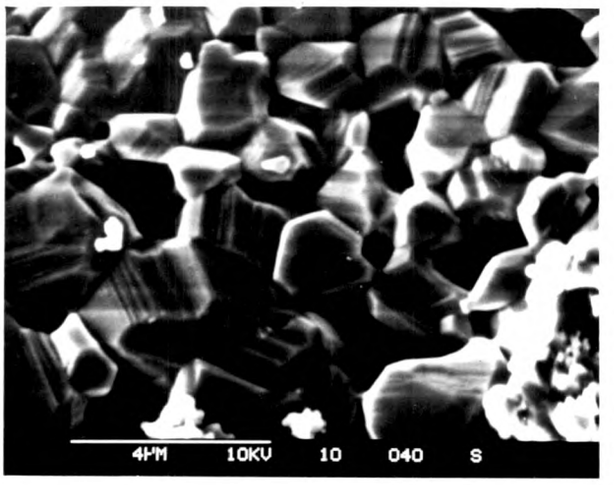

B_4

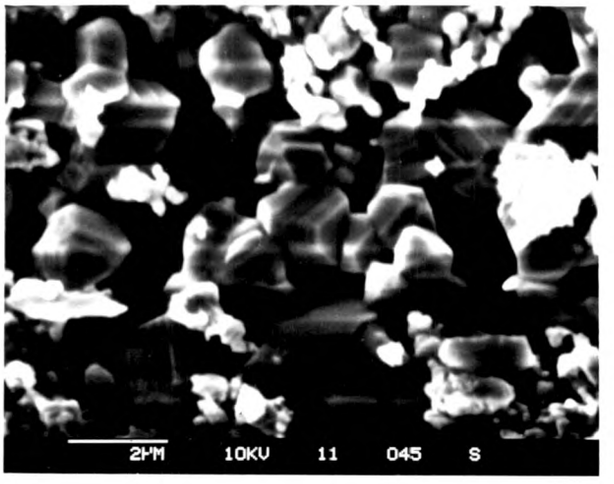

B_5

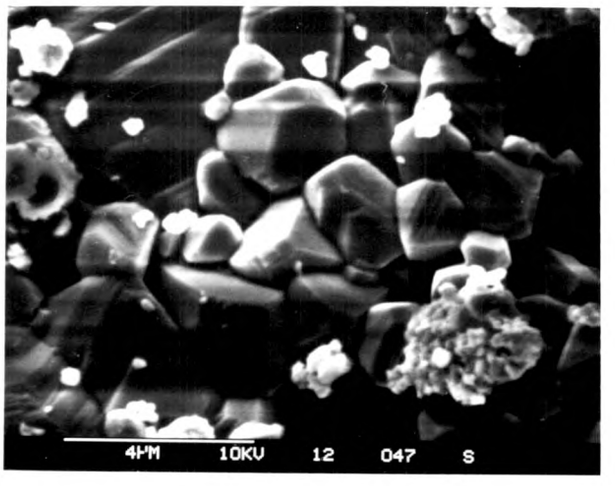

B_6

Fig. 3.10(b)

MICROGRAPHS OF SAMPLES B_4, B_5 AND B_6

3. From B_4 to B_6, the variation of porosity is observed significantly in the micrographs.

4. The segregation of impurity phases at the grain boundaries is observed for B_5 and B_6 and amount of segregation increases in B_6.

5. No intragranular porosity is observed in the presented micrographs.

The group at NPL,[50-53] has studied the effect of substituents like SiO_2, GeO_2, V_2O_5 and CaO on grain growth kinetics of Mn-Zn and Ni-Zn ferrites which are prepared, using standard ceramic - technique. They have concluded that upto the solid solubility limit, the grains grow normally as decided by oxygen-ion vacancy concentration, just beyond the solid solubility limit discontinuous grain growth with lot of intragranular porosity occurs and at higher concentrations, grains again become regular with a few - intragranular pores and a second phase present at grain boundaries and corners. The similar behaviour of normal grain growth is - observed upto B_3 and secondary phases begin at the grain boundaries. The exaggerated grain growth and intragranular pores are - not observed. The modification in the microstructure may be due to Mn in the present system.

Some factors such as permeability and losses are depenient mostly on the microstructural conditions. Effect of grain size - on permeability was studied by Guillaud and Paulus on Ni-Zn ferrites, Beer and Schartz and Roess on Mn-Zn ferrites.[54] They have - observed the increase in permeability with increase of grain diameter but this may not be true because grain size alone is not an important factor for high permeability. Other imperfections -

limiting the moment of domain walls are pores. A problem encountered in growing large grains in ferrites is that during the course of growing large grains many pores are swept over by the grain boundary and remain inside, the large grain. The intragranular porosity is more troublesome than the intergranular. Guillaud has observed the similar behaviour in Ni-Zn ferrites.

Ross et al[55] have found that an increase in permeability with grain size is primarily caused by decrease in the internal stresses in the material. But this is true only when the crystalline anisotropy is very low. In regions where this anisotropy has a finite value, the permeability can even decrease with increase in grain diameter. In our samples, the permeability decreases as the grain-size increases upto 0.1 as in table 3.5. This may be due to anisotropy constant. Globus has given the relation, $\mu i = M_s^2 .dm/K_1$ where μi = initial permeability, dm = average grain diameter and K_1 = anisotropy constant. So, depending on the Ms and K_1, the permeability changes.

In addition to grain boundaries and pores, there are ceramic imperfections that can impede domain wall motion and these reduce the permeability. These include pores, cracks, inclusions and second phases as well as residual strains.

For doped samples, initial permeability increases with that of grain size upto 0.1 content of Mn, and then it decreases with decrease of grain size for higher concentrations of Mn. Variations of initial permeability and resistivity with Mn content are shown in figure 3.11. The variation is not systematic with Mn content. Microstructural modifications by retarding secondary grain growth and segregation of phases at grain boundary are believed to be the causes of such variations.[56]

TABLE 3.5

AVERAGE GRAIN DIAMETER AND PERMEABILITY VALUES FOR DIFFERENT COMPOSITIONS

Sample	Average Grain diameter in M	Initial Permeability at room temperature for 1 KHz.
B_1	0.8615	128.6
B_2	1.4446	72.8
B_3	1.5359	79.55
B_4	1.4826	42.95
B_5	1.1667	31.27
B_6	1.2783	27.10

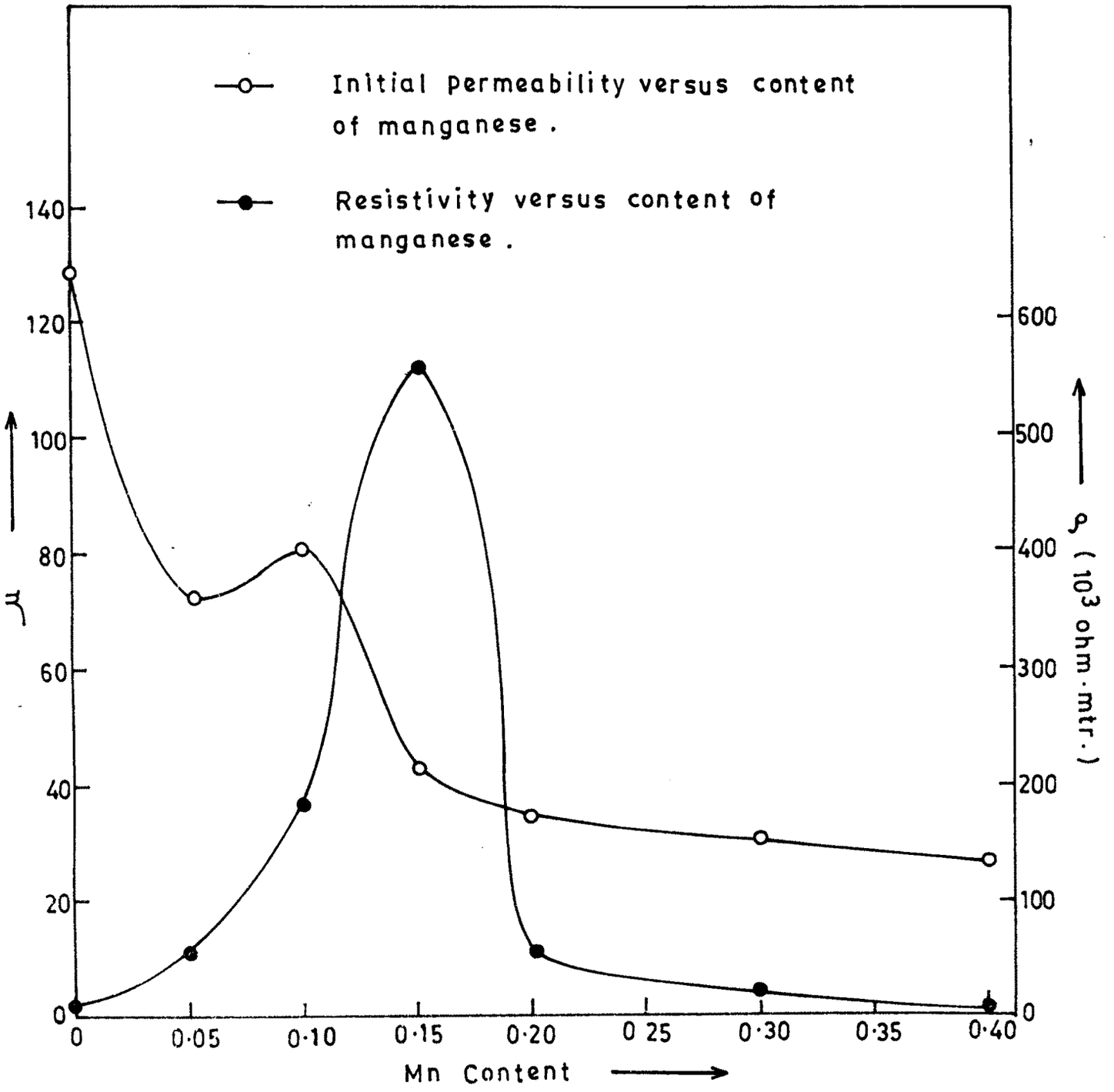
Initial permeability versus content of manganese .
Resistivity versus content of manganese .
140
120
100
80
60
40
20
0
μ
600
500
400
300
200
100
0
ρ (10³ ohm·mtr.)
0
0·05
0·10
0·15
0·20
0 25
0·30
0·35
0·40
Mn Content

FIG. 3·11

REFERENCES

1. Weiss P. J.Phy. Theo. Appl. 6 667 (1907).
2. Heisenberg.W. Z.Phys. 49, 619 (1978).
3. Neel L. Ann.Phy.(Paris) 3, 137 (1948).
4. Kramers H.A. Physica. 1, 182 (1934).
5. Anderson P.W. Phy. Rev. 79, 350 (1950).
6. Alex Goldman. "Electronic Ceramics, Prop. devices and Applications. Ed. Lionel M Levinson, N.Y. (1988).
7. Alper A.M. 'High Temperature Oxides'. Acad. Press New York. (N.Y)(1971).
8. Pakhomova N.L. and V.Christoph: Phys. Stat. Soli (a) 103, (1987).
9. Das A.R, V.S.Ananthan and D.C.Khan. J. Appl. Phys. 57(1) (1985).
10. Jadhav.S.R, S.R.Sawant, S.S.Suryawanshi and S.A.Patil. J. less Common metals. 158, 199-205 (1990).
11. Gorter E.W. Phillips Res. Rept. 9 295(1954).
12. Hiroshi Yasouka, Akira Hirai; T.Shinjo, M.Kiyama, Y.Bando and T.Takada. J.Phy. Soc. of Japan 22 (1) (1967).
13. Patil.S.A, C.N.Jadhav, S.S.Suryawanshi, S.R.Sawant and R.N.Patil. ICEM. 90 Sept.17-19, Newark New Jersey USA, (1990).
14. Kishan.P., C.Prakash, J.S.Baijal, K.K.Laroia. Phy. Stat. Sol. (a) 84, 535 (1984).
15. Puri R.K, Vijay K. Babbar, R.G.Mendiratta. Proc. ICF 5- 239-243, (1989).
16. Rezlescu N, Istrate S, Rezlescu E and Luca E. J. Phy. Chem. Solids. 35 (1974).

17 Laroia K.K. and Sinha A.P.B.
Ind. J. Pure and Applied Phys. 1, 215 (1963).

18 Maxwell and Pickart loc. Cit.

19 Van Uitert L.G. Low Mag. Sat. Ferrites for Microwave Applications. J. Appl. Phy. 26, 1289 (1955).

20 Lax and Button 'Ferrimagnetic Oxides'. P.121.

21 Haug M, M.Fahnle, H.Kronmuller and Habery.
J. Mag.and Mag. Mat. 69, 163 (1987).

22 Beer A and T.Schwartz.IEEE. Trans. Magnet. 2, 470,(1966).

23 Perduijn and Peloschek.
Proc. Brit. Ceram. Soc. 10, 263 (1968).

24 Roess Angew. Phys. 21, 391 (1966).

25 Guillaud C. and M.Paulaus. C.R. 230, 1458 (1950).

26 Guillaud C. Proc. IEEE 104-B,165 (1957).

27 Fomenko G.V. and Bashkieve L.A. Izvestiya Akademii Nauk. USSR Neogra nicheskia Materialy 18, 1886 (1982).

28 Rado G.T. and Terris Phy. Rev. 83, 177 (1951).

29 Stopples D. Philips. Res. Lab. Netherlands.
J. Appl. Phy. 52(3), 2433 (1981).

30 Buck D. and E.Ross. Phys. Stat. Soli. 32, 659 (1969).

31 Globus A. IEEE. Trans. on Mag. Mag.-7, 617 (1971).

32 Standley K.J. 'Oxide Magnetic Materials'.
Clarendon. Oxford P.98, (1972).

33 Varshney U. and R.J.Churchill in Proc. ICF 5, (1989).

34 Heister W.J. Phy. Appl. 30, 225 (1959).

35 Paulus M. Phy. Stat. Sol. 2, 1181 and 1325 (1962).

36 Guillaud.C; Paulus M. C.R.Acad. Sc. 242, 2525 (1956).

37 Van Uitert L.G. Proc. I.R.E. 44, 10 (1956).

38 Longkla S., Tein-Shouwu, Chang-Chang Wei.
J. Phy. D. (4B) 13/2, D-259, (1980).

39 Bosman A.J, Crevecoeur C. Phy. Rev. 144(2), 763 (1966).

40 Jong Tae Baek Su.Il Pyan Hobin Im.
J.Korean Phy. Soc. Vol.16, No.1, P.97-104 (1983).

41 Perduijn D.J. and Peloschek H.P.
Proc. Brit. Ceram. Soc. 10, 263 (1968).

42 Igarashi H.,Okazaki K.
J. Am. Ceram. Soc. (USA) 60,(1-2), 51 (1977).

43 Besenicar S, Hanzel D.
J. Phy. Colloq.(France) 46 (C6),169 (1985).

44 Burke J.E. in "Kinetics of High Temp. Processes."
Ed. W.D. Kingeri (N.Y), P.109 (1959).

45 Reijnen J.L. Sci. Ceram. 4, 169 (1968).

46 Nabarrow F.R.N. Rep. Conf. Strength of solids.
Phys. Soc. London.P.75 (1948).

47 Herring C. J.Appl. Phy. 21, 437 (1950).

48 Paulus M.J. and Hamelin A.
J.Cry. Growth. 3, 500 (1968).

49 Beek P.A, Halzworth M.C. and Sperry P.
Trans. AMIE 180, 163 (1949).

50 Jain G.C, Das B.K., Kumari.S.
IEEE. Tran. on Mag. Mag. 12, 1428 (1980).

51 Jain G.C, Das B.K. and Kumari S. J. Appl.Phy. 49, 2894(1978).

52 Narayan R. Ph.D. Thesis. Delhi University. (1980).

53 Goel N.C. Ph.D. Thesis. Delhi University. (1971).

54 Alex Goldman. Electronic Ceramics, Properties, devices and applications. Ed: Lionel M.Levinson. Marcell Dekker Inc. N.Y. (1988).

55 Das B.K. 'Preparation and Characterisation of Materials.' P.75-100.
Ed: J.M.Honig, CNR.Rao. Acad. Press. N.Y. (1981).